Supporting Information for

Modulating W^{5+}/W^{6+} in $PtCu/WO_x$ Schottky Heterojunctions for Optimized Built-in Electric Field to Accelerate the Oxygen Reduction Reaction

*Jiaqing Liu,† Xinran Sun,† Jilan Zeng, Jiayi Chen, Sibo Wang, and Xue Feng Lu**

J. Liu, X. Sun, J. Zeng, J. Chen, S. Wang, X. F. Lu

State Key Laboratory of Chemistry for NBC Hazards Protection, State Key Laboratory of Photocatalysis on Energy and Environment, College of Chemistry, Fuzhou University, Fuzhou 350116, China

E-mail: luxf@fzu.edu.cn

† These authors contribute equally to this work.

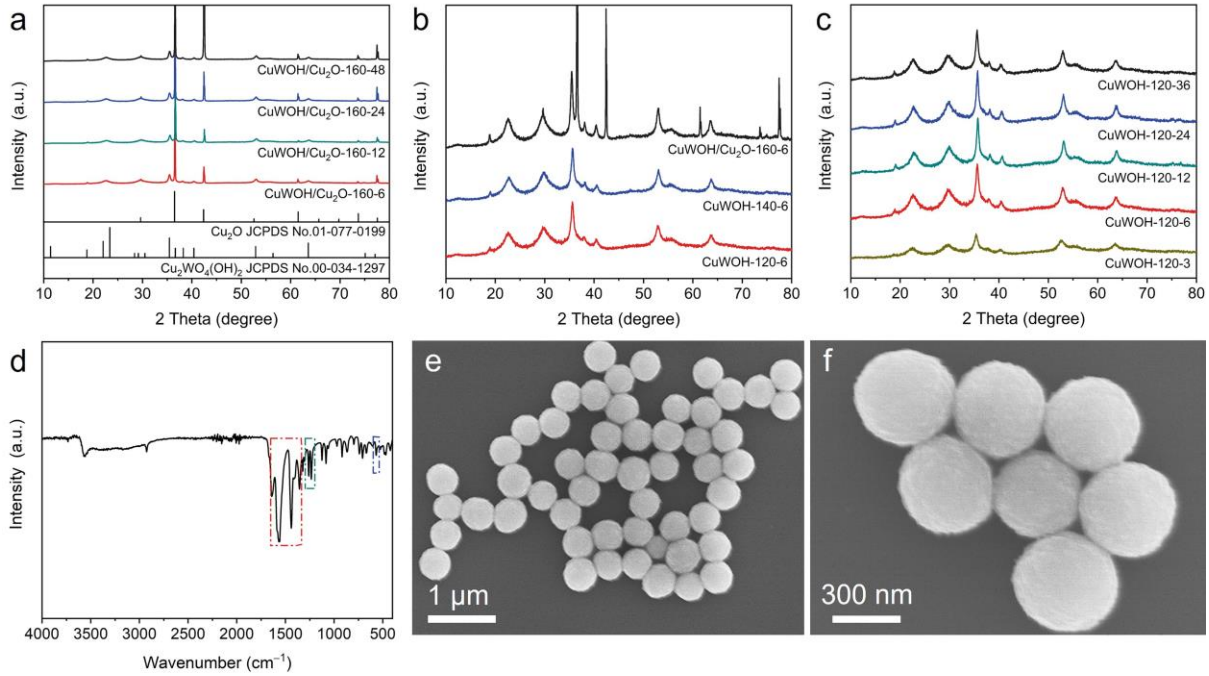

Supplementary Fig.1 | Characterization of CuWOH. a-c XRD patterns, **d** FTIR spectrum, and **e,f** SEM images of CuWOH.

$Cu_2WO_4(OH)_2$ microspheres (CuWOH) were successfully synthesized but contained Cu_2O impurities (Supplementary Fig. 1a). To provide valuable references for the synthesis of single CuWOH and mitigate potential interference of phase-separated Cu_2O in subsequent experiments, a comprehensive investigation of the synthesis process is imperative. Based on the inherent properties of sodium citrate and previous studies, it is speculated that under high temperature and pressure conditions, the hydroxyl groups in citrate could exhibit reducibility, which facilitates chelation of free or unstable Cu^{2+} ions into Cu^{1+}, ultimately forming Cu_2O precipitates.[1,2,3,4] To validate this hypothesis, the reaction time was varied while maintaining a constant reaction temperature, and intense diffraction peaks corresponding to Cu_2O were observed regardless (Supplementary Fig. 1a). This result suggests that the reducibility of hydroxyl groups in citrate is not fundamentally influenced by the reaction time. Conversely, when the reaction temperature was reduced while keeping a fixed reaction time, effective suppression of Cu_2O formation was achieved, providing compelling evidence that reaction temperature plays a pivotal role in regulating the

reducibility of hydroxyl groups within citrate (Supplementary Fig.1b). Therefore, at a fixed reaction temperature of 120°C, no Cu_2O particles were observed regardless of the variation in reaction time, which substantiates the hypothesis (Supplementary Fig.1c). Taking into account both energy conservation and production efficiency, CuWOH was successfully synthesized under optimized conditions of a fixed reaction temperature at 120°C and a reaction time of 6 hours. The functional groups on the CuWOH surface were further verified by FTIR, where the anti-symmetric vibrational peaks of COO^- in copper citrate are observed at 1638 and 1565 cm^{-1}, while the symmetric vibrational peaks are detected at 1439 and 1355 cm^{-1} (Supplementary Fig.1d). The deformation vibrations of C–OH can be identified by the peaks at 1260 and 1232 cm^{-1}. Furthermore, the stretching vibration of Cu–O is indicated by the peak at 567 cm^{-1}, providing evidence for the successful synthesis of CuWOH. SEM images show that the CuWOH consists of solid spheres with smooth surfaces and clear boundaries (Supplementary Fig.1e,f).

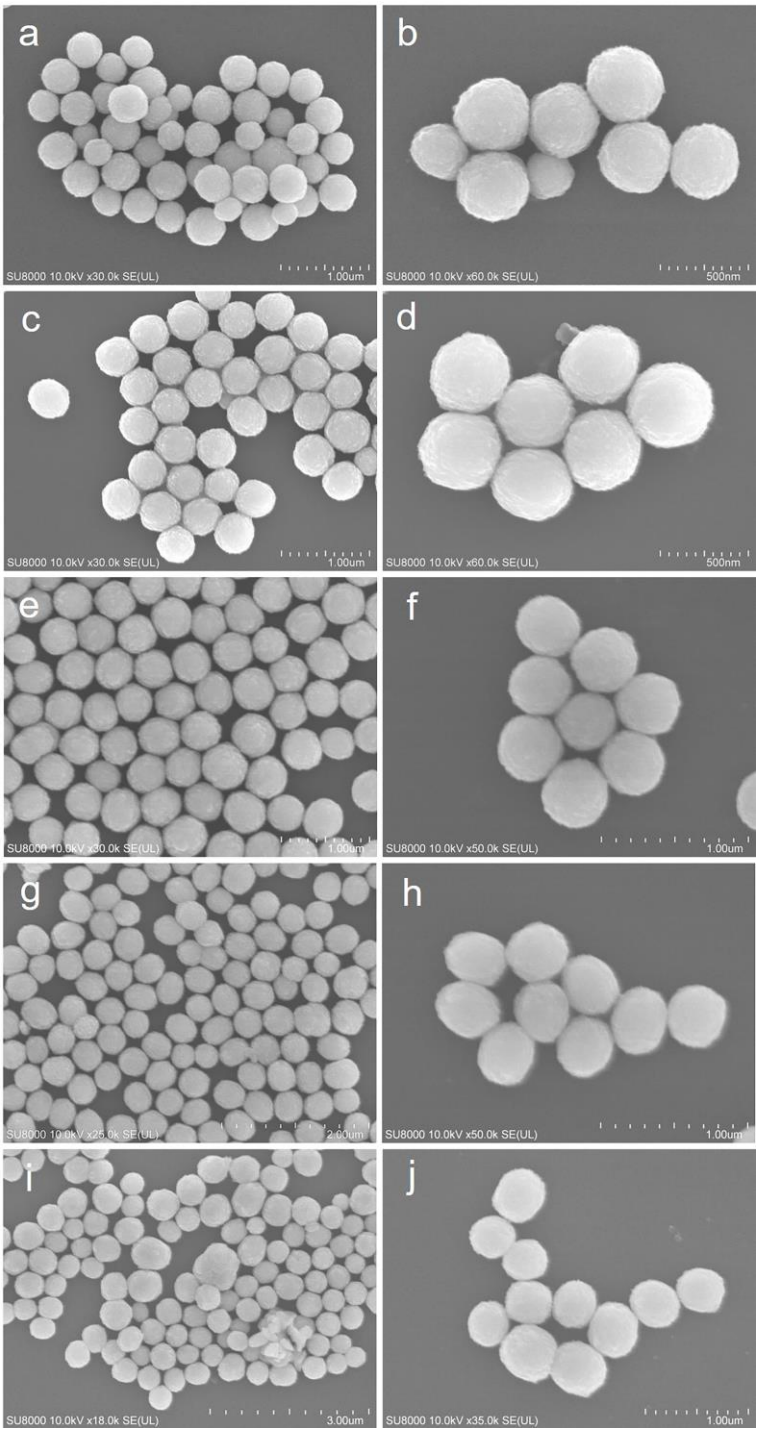

Supplementary Fig.2 | Morphology characterization of CuWOH. SEM images of CuWOH at 120°C with different reaction times: a,b) 3 h, c,d) 6 h, e,f) 12 h, g,h) 24 h, and i,j) 36 h.

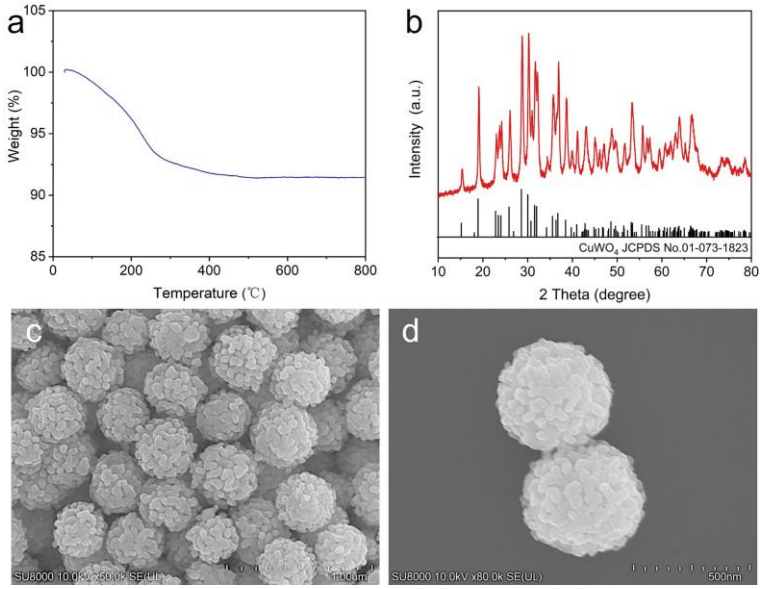

Supplementary Fig.3 | Morphology and composition characterization of $CuWO_4$. a) TGA spectrum of CuWOH in air atmosphere. b) XRD patterns and c,d) SEM images of $CuWO_4$.

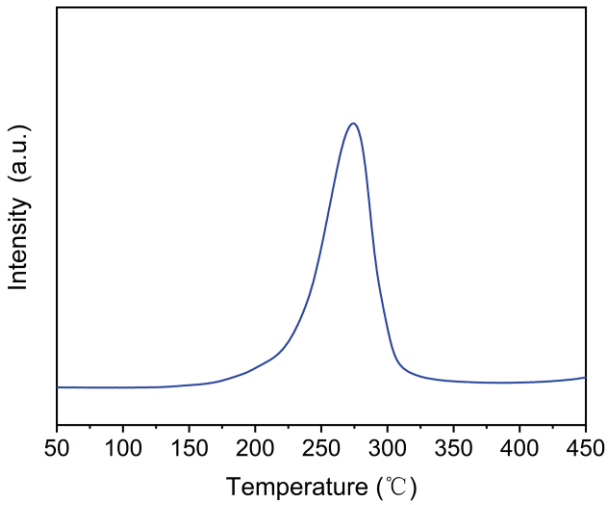

Supplementary Fig.4 | CuWOH reduction. H_2-TPR spectrum of $CuWO_4$.

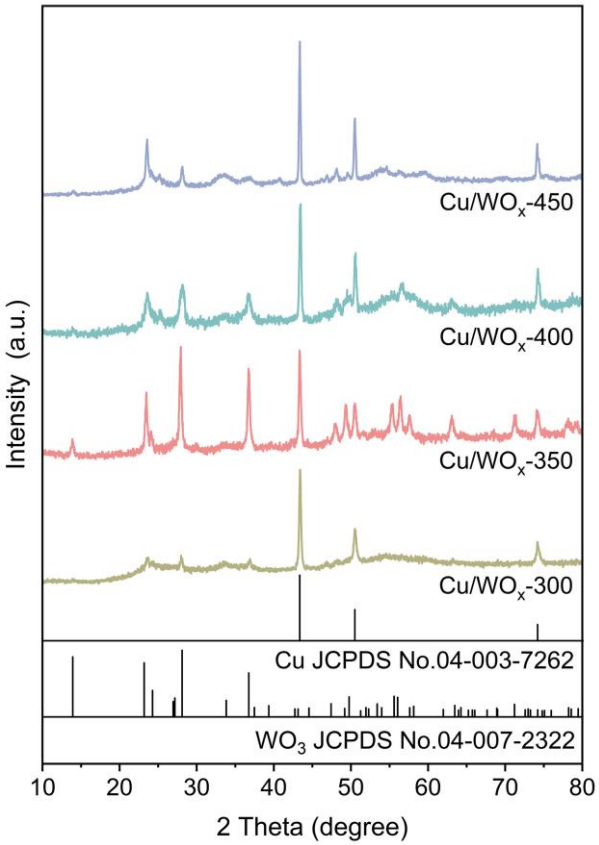

Supplementary Fig.5 | Phase structure of Cu/WO$_x$. XRD patterns of Cu/WO$_x$.

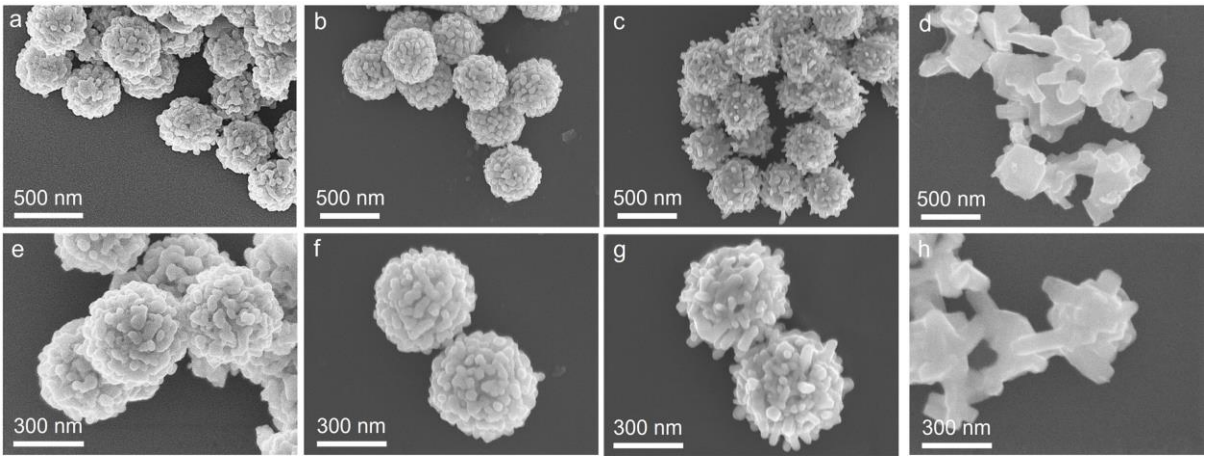

Supplementary Fig.6 | Morphology of Cu/WO$_x$. SEM images of a,e) Cu/WO$_x$-300, b,f) Cu/WO$_x$-350, c,g) Cu/WO$_x$-400, and d,h) Cu/WO$_x$-450.

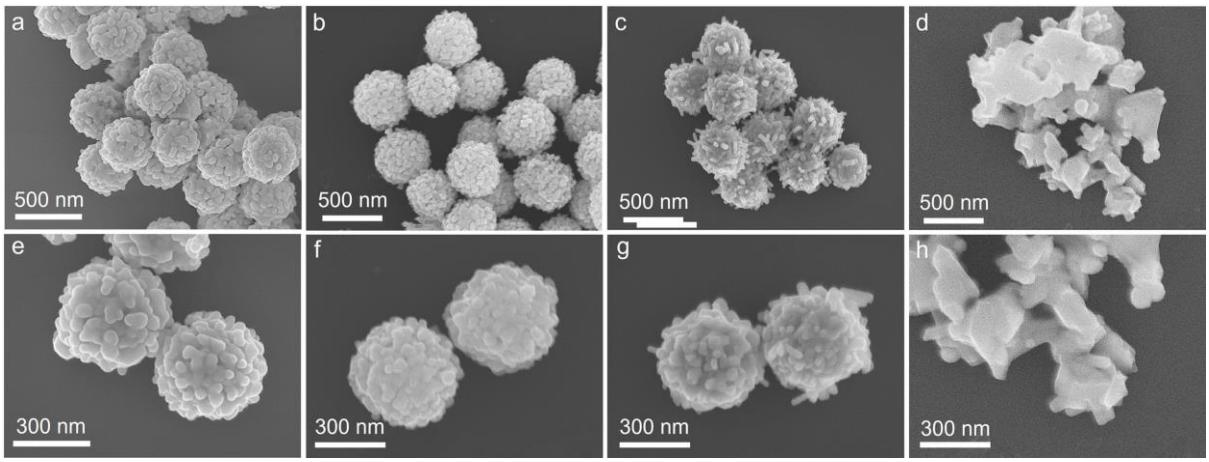

Supplementary Fig.7 | Morphology of PtCu/WO$_x$. SEM images of a,e) PtCu/WO$_x$-300, b,f) PtCu/WO$_x$-350, c,g) PtCu/WO$_x$-400, and d,h) PtCu/WO$_x$-450.

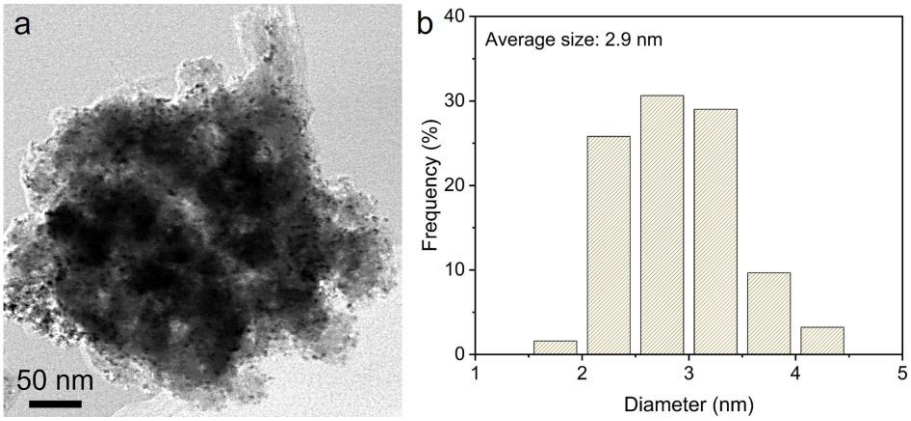

Supplementary Fig.8 | Size distribution of PtCu in PtCu/WO$_x$-350. a) TEM image of PtCu/WO$_x$-350. b) Size distribution of PtCu alloy particles.

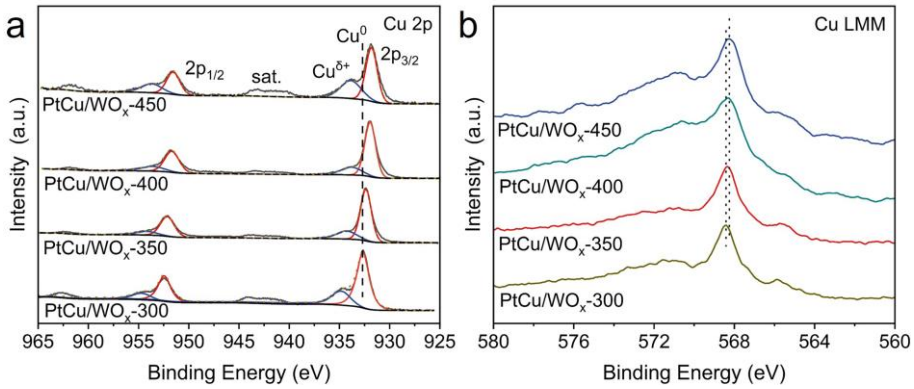

Supplementary Fig.9 | Electronic structure of PtCu/WO$_x$. High-resolution XPS spectra of a) Cu 2p, and b) Cu LMM for PtCu/WO$_x$.

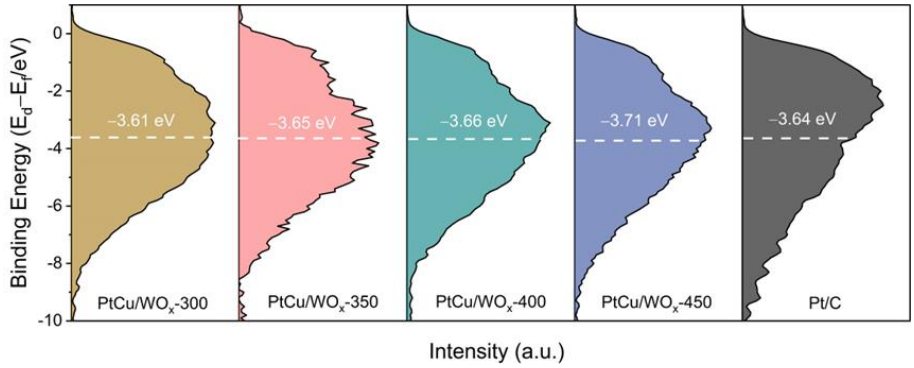

Supplementary Fig.10 | Electronic structure of PtCu/WO$_x$. XPS-VB spectra of PtCu/WO$_x$.

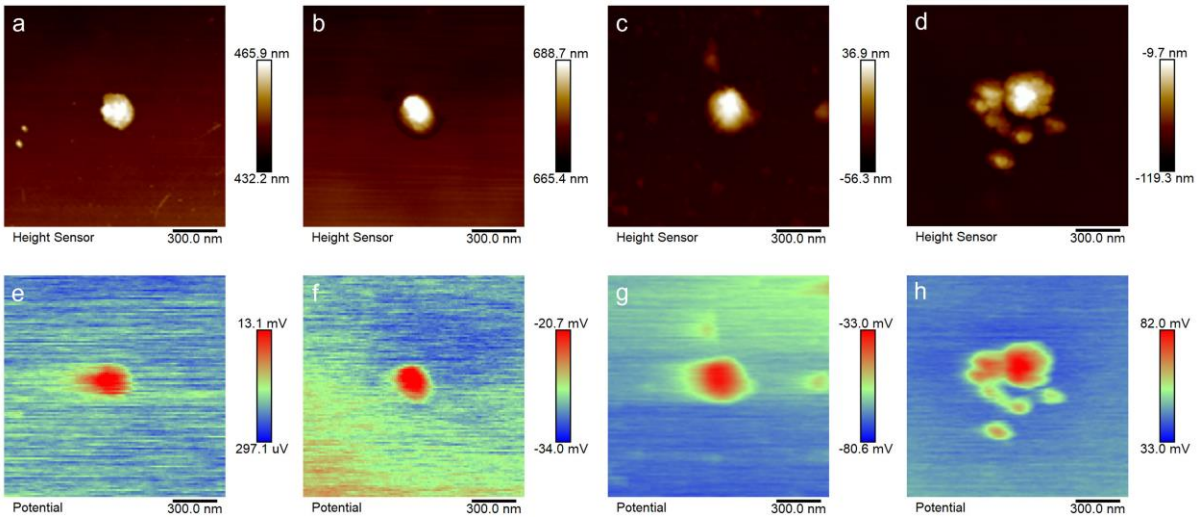

Supplementary Fig.11 | BIEF and morphological characterization of PtCu/WO$_x$. AFM and KPFM images for a,e) PtCu/WO$_x$-300, b,f) PtCu/WO$_x$-350, c,g) PtCu/WO$_x$-400, and d,h) PtCu/WO$_x$-450.

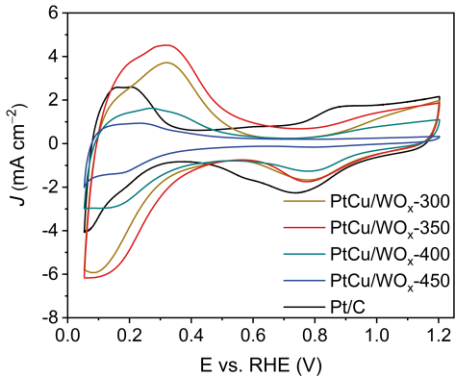

Supplementary Fig.12 | ECSA Characterization of PtCu/WOx. CV curves of PtCu/WOx in N_2-saturated 0.1 M $HClO_4$.

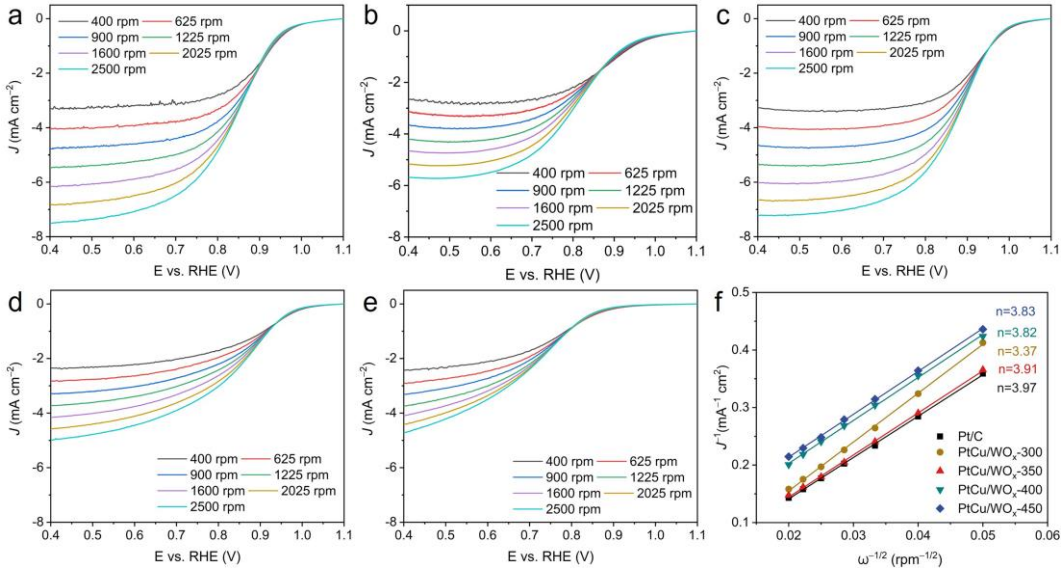

Supplementary Fig.13 | Kinetic characterization of PtCu/WOx. LSV curves on RDE in O_2-saturated 0.1 M $HClO_4$ at different rotation speeds from 400 to 2500 rpm at a scan rate of 10 mV s^{-1} in ORR region: a) Pt/C, b) PtCu/WOx-300, c) PtCu/WOx-350, d) PtCu/WOx-400, e) PtCu/WOx-450, and f) Koutecký-Levich plots at 0.4 V vs. RHE.

Supplementary Table 1 | Mass percentage and molar ratio of Pt and Cu in different samples.

	$PtCu/WO_x$-300	$PtCu/WO_x$-350	$PtCu/WO_x$-400	$PtCu/WO_x$-450
Pt (wt %)	20.71	19.75	18.45	18.13
Cu (wt %)	10.69	10.23	8.65	9.28
Molar ratio (Pt/Cu)	1.58	1.59	1.44	1.57

Supplementary Table 2 | The ORR activity of $PtCu/WO_x$ compared with other Pt-based catalysts.

Catalysts	Electrolyte	$E_{1/2}$ (V vs. RHE)	Ref.
$PtCu/WO_x$-300	0.1 M $HClO_4$	0.83	This work
$PtCu/WO_x$-350	0.1 M $HClO_4$	0.89	This work
$PtCu/WO_x$-400	0.1 M $HClO_4$	0.85	This work
$PtCu/WO_x$-450	0.1 M $HClO_4$	0.72	This work
Pt_1Fe_1@$Fe_{0.5}$NC-900	0.1 M $HClO_4$	0.889	5
$PtCu_1$-NC	0.1 M $HClO_4$	0.890	6
$Pt1Co_{100}$/N-GCNT	0.1 M $HClO_4$	0.85	7
Vac-NiPt NPs/NG	0.1 M $HClO_4$	0.901	8
PtFe/M-700	0.1 M $HClO_4$	0.938	9
20 wt% Pt/d-$Ti_{0.9}Mo_{0.1}O_y$	0.5 M H_2SO_4	0.84	10
WO_x–PtNi NWs	0.1 M $HClO_4$	0.93	11
Pt NPs/TiO_2 NRs	0.1 M $HClO_4$	0.86	12
Pt/black WO_{3-x} NFs	0.1 M $HClO_4$	0.85	[1]3
Pt/UMTHS	0.1 M $HClO_4$	0.867	14

References

1. Hu J-Q*, et al.* A Simple and Effective Route for the Synthesis of Crystalline Silver Nanorods and Nanowires. *Adv Funct Mater* **14**, 183-189 (2004).
2. Caswell KK, Bender CM, Murphy CJ. Seedless, Surfactantless Wet Chemical Synthesis of Silver Nanowires. *Nano Lett* **3**, 667-669 (2003).
3. Brown KR, Walter DG, Natan MJ. Seeding of Colloidal Au Nanoparticle Solutions. 2. Improved Control of Particle Size and Shape. *Chem Mater* **12**, 306-313 (2000).
4. Liu Y, Male KB, Bouvrette P, Luong JHT. Control of the Size and Distribution of Gold Nanoparticles by Unmodified Cyclodextrins. *Chem Mater* **15**, 4172-4180 (2003).
5. Wu Y*, et al.* Ptfe Nanoalloys Supported on Fe - Based Cubic Framework as Efficient Oxygen Reduction Electrocatalysts for Proton Exchange Membrane Fuel Cells. *Adv Funct Mater* **34**, 2307297 (2024).
6. Li M, Liu F, Zhang Y. Synergistic Effect of Electrocatalyst for Enhanced Oxygen Reduction Reaction: Low Pt-Loaded Cupt Alloy Nanoparticles Supported on N-Doped Hierarchical Porous Carbon. *ACS Appl Mater Interfaces* **16**, 13893-13902 (2024).
7. Cheng X*, et al.* Single-Atom Alloy with Pt-Co Dual Sites as an Efficient Electrocatalyst for Oxygen Reduction Reaction. *Appl Catal, B* **306**, 121112 (2022).
8. Ye S*, et al.* Harnessing the Synergistic Interplay between Atomic-Scale Vacancies and Ligand Effect to Optimize the Oxygen Reduction Activity and Tolerance Performance. *Angew Chem Int Ed* **64**, e202414989 (2025).
9. Zhang Y, Zhao Q, Danil B, Xiao W, Yang X. Oxygen - Vacancy - Induced Formation of Pt - Based Intermetallics on Mxene with Strong Metal - Support Interactions for Efficient Oxygen Reduction Reaction. *Adv Mater* **36**, 2400198 (2024).
10. Tsai M-C*, et al.* Interplay between Molybdenum Dopant and Oxygen Vacancies in a TiO2 Support Enhances the Oxygen Reduction Reaction. *ACS Catal* **6**, 6551-6559 (2016).
11. Mo Y*, et al.* Surface Unsaturated Wox Activating Ptni Alloy Nanowires for Oxygen Reduction Reaction. *J Colloid Interface Sci* **607**, 1928-1935 (2022).
12. Kumar PSM*, et al.* Controlled Synthesis of Pt Nanoparticle Supported Tio 2 Nanorods as Efficient and Stable Electrocatalysts for the Oxygen Reduction Reaction. *J Mater Chem A* **6**, 23435-23444 (2018).
13. Kim GY, Yoon KR, Shin K, Jung JW, Henkelman G, Ryu WH. Black Tungsten Oxide Nanofiber as a Robust Support for Metal Catalysts: High Catalyst Loading for Electrochemical Oxygen Reduction. *Small* **17**, 2103755 (2021).
14. He S*, et al.* Uniform Pt Nanoparticles Supported on Urchin-Like Mesoporous Tio 2 Hollow Spheres as Stable Electrocatalysts for the Oxygen Reduction Reaction. *Nanoscale* **12**, 10656-10663 (2020).